

Constraints on Majorana Dark Matter from the LHC and IceCube

Jan Heisig^{1*}, Michael Krämer^{1†}, Mathieu Pellen^{1‡}, Christopher Wiebusch^{2§}

¹*Institute for Theoretical Particle Physics and Cosmology,
RWTH Aachen University, 52056 Aachen, Germany*

² *III. Physikalisches Institut B, RWTH Aachen University, 52056 Aachen, Germany*

September 2015

Abstract

We consider a simplified model for Majorana fermion dark matter and explore constraints from direct, indirect and LHC collider searches. The dark matter is assumed to couple to the Standard Model through a vector mediator with axial-vector interactions. We provide detailed analyses of LHC mono-jet searches and IceCube limits on dark matter annihilation in the Sun. In particular, we develop a method for calculating limits on simplified WIMP dark matter models from public IceCube data, which are only available for a limited number of Standard Model final states. We demonstrate that LHC and IceCube searches for Majorana dark matter are complementary and derive new limits on the dark matter and mediator masses, including in addition constraints from LHC di-jet searches, direct detection and the dark matter relic density.

*E-mail: heisig@physik.rwth-aachen.de

†E-mail: mkraemer@physik.rwth-aachen.de

‡E-mail: pellen@physik.rwth-aachen.de

§E-mail: wiebusch@physik.rwth-aachen.de

Contents

1	Introduction	1
2	A simplified model for Majorana fermion dark matter	2
3	Collider limits	3
3.1	Mono-jet limits	3
3.2	Di-jet limits	6
4	Astrophysical and cosmological constraints	6
4.1	Relic density	6
4.2	Limits from IceCube	7
4.2.1	Limit on σ_{SD} for annihilation into $t\bar{t}$	8
4.2.2	Limit on σ_{SD} for annihilation into VV	9
4.2.3	Equilibrium condition for capturing and annihilation in the Sun	10
4.3	Limits from direct detection	12
5	Results and Discussion	12
6	Conclusion	14
	References	14

1 Introduction

Weakly interacting massive particles (WIMPs) are attractive candidates for dark matter and are predicted by various extensions of the Standard Model (SM). Searches for WIMPs at the Large Hadron Collider (LHC) and through direct and indirect detection experiments are complementary, and probe different types of dark matter models and different regions of the model parameter space.

To explore the nature of dark matter, and to be able to combine results from direct, indirect and collider searches, one may follow a more model-independent approach. So-called simplified models (see *e.g.* [1–3] and references therein) describe dark matter and its experimental signatures with a minimal amount of new particles, interactions and model parameters. They thus allow us to explore the landscape of dark matter theories, and serve as a mediator between the experimental searches and more complete theories of dark matter.

Many simplified models for dark matter have been proposed in the literature. Minimal models describe dark matter by a single particle which interacts with the SM through a single mediator. We focus on a model with Majorana fermion dark matter and a vector mediator with axial-vector couplings to quarks. Such models predict spin-dependent WIMP-nucleon scattering cross sections and can thus be probed by IceCube in the search for dark matter annihilation in the Sun [4, 5]. Previous work on dark matter models with (axial-)vector mediators [6–10] has mainly focused on Dirac fermion dark matter and, in particular, has not analyzed dark matter limits from IceCube.

The complementarity of IceCube and LHC searches for dark matter has been explored in Ref. [4], albeit in an effective field theory (EFT) approach, where the masses of all particles mediating the interaction between the SM and dark matter are assumed to be large compared to the energy scale of the process. The EFT limit is reliable to interpret the low-energy WIMP-nucleon interactions which are probed by direct detection experiments, but it may break down when analyzing dark matter searches with IceCube and with the LHC. While the capture of

WIMPs in the Sun is well described by an EFT, the annihilation process is in general not. Indeed, as we will show, the IceCube limits are sensitive to details of the simplified model which cannot be described within the EFT. Furthermore, the EFT may break down when probing dark matter production at the LHC: when the energy scale of the interaction is near or larger than the mass of the mediator, resonance effects become important, and the mediator has to be included in the particle spectrum of the model [11–20].

We thus provide a comprehensive analysis of collider, direct and indirect detection constraints on Majorana dark matter with vector mediators in the simplified model framework. The paper is organized as follows. The dark matter model is introduced in section 2. We derive limits on the model parameters from LHC searches in section 3. In particular, we use the most recent results for mono-jet searches from both the ATLAS [21] and CMS [22] collaborations. Section 4 addresses constraints from the dark matter relic density, from direct dark matter searches, and, in particular, searches for dark matter annihilation in the Sun with IceCube. For a mediator that is lighter than the WIMP, annihilation into a pair of mediators can be dominant. In order to determine the IceCube model rejection factor in this region of parameter space we develop a method to estimate the limits for annihilation into two mediators on the basis of the limits for annihilation into the SM particles the mediator decays into. We validate this method by applying it to annihilation into top quark pairs for which we find very good agreement with the most recent public IceCube dark matter annihilation limits [23] for that channel. We finally combine the various constraints and derive new limits on the dark matter and mediator masses in section 5. Our conclusions are presented in section 6.

2 A simplified model for Majorana fermion dark matter

We focus on a minimal model with Majorana fermion dark matter, χ , and a vector mediator, V_μ , with axial-vector couplings to quarks,

$$\mathcal{L} \supset g_\chi \bar{\chi} \gamma^\mu \gamma^5 \chi V_\mu + g_q \bar{q} \gamma^\mu \gamma^5 q V_\mu. \quad (1)$$

We assume universal couplings of the mediator to the SM quarks and neglect couplings to leptons.¹ Thus the model has only four independent parameters: the couplings of the mediator to the dark matter and the SM quarks, g_χ , and g_q , and the dark matter and mediator masses, m_χ and M_V , respectively. We require both couplings to be $g_\chi, g_q < 4\pi$.

The axial-vector interaction of Majorana dark matter with nuclei leads to spin-dependent scattering cross sections and contributes significantly to the dark matter capture rate in the Sun (see section 4.2). Searching for dark matter annihilation in the Sun with the neutrino telescope IceCube can thus place strong limits on such models, which are competitive with direct detection bounds and with dark matter searches at the LHC.

The width of the mediator, Γ_V , is determined by the particle masses and the couplings:

$$\Gamma_V = \frac{M_V}{\pi} \left(\frac{g_\chi^2}{6} \left(1 - 4 \frac{m_\chi^2}{M_V^2} \right)^{3/2} + \sum_{i=1}^6 \frac{g_q^2}{4} \left(1 - 4 \frac{m_{q_i}^2}{M_V^2} \right)^{3/2} \right), \quad (2)$$

where m_{q_i} is the mass of the SM quarks.

The dark matter cross section at the LHC and the WIMP-nucleon scattering cross section depend on the product of the couplings and on the width of the mediator, $\sqrt{g_q g_\chi}$ and Γ_V , respectively. We will thus present our results in terms of Γ_V and $\sqrt{g_q g_\chi}$, rather than in terms of the individual couplings g_q and g_χ .

¹The case of different couplings to up- and down-type quarks has been considered *e.g.* in Ref. [10]. However, as discussed in Ref. [24], gauge-invariance sets very tight constraints on the difference of these couplings.

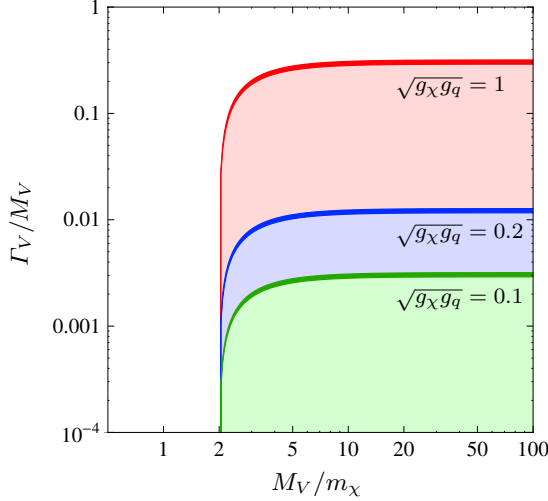


Figure 1: Non-accessible regions in the M_V/m_χ - Γ_V/M_V plane for $\sqrt{g_\chi g_q} = 1$ (red shaded region), 0.2 (blue shaded region) and 0.1 (green shaded region). The width of the bands marking the boundaries of the shaded regions indicates the explicit dependence on m_χ : the upper and lower edge of the band correspond to the boundaries for $m_\chi = 1$ TeV and 1 GeV, respectively.

The relation between Γ_V , $\sqrt{g_q g_\chi}$ and the individual couplings g_q and g_χ provides some insight into the phenomenology of this model. In the region $M_V > 2m_\chi$, and for any given value of the product of the couplings, $\sqrt{g_q g_\chi}$, we encounter a minimal value for the mediator width, below which there is no solution for the individual couplings within the model. These regions are shown in Fig. 1 in the M_V/m_χ - Γ_V/M_V plane. The inaccessible regions only depend very mildly on m_χ , as indicated by the width of the bands marking the boundaries of the shaded regions (here m_χ was varied between 1 GeV and 1 TeV). In the allowed part of the region where $M_V > 2m_\chi$ there exist two solutions for g_q for any given $\sqrt{g_q g_\chi}$. To derive conservative limits on the model from di-jet production (see Sec. 3.2), we adopt the smaller value for g_q in our analysis, unless this would cause $g_\chi > 4\pi$ for a given $\sqrt{g_q g_\chi}$.

In the EFT limit $M_V \gg m_\chi$, where dark matter and SM quarks interact through a 4-fermion operator with coefficient $1/M_*^2 = g_q g_\chi / M_V^2$, we find that $\Gamma_V/M_V \gtrsim 0.3 g_\chi g_q = 0.3 (M_V/M_*)^2$. The LHC Run I data probe suppression scales $M_* \lesssim 1$ TeV, see Sec. 3. Thus, in the region $M_V \gg \sqrt{s}$ where the EFT is valid, Γ_V/M_V is typically larger than one, inconsistent with a particle-like interpretation of the mediator (*cf.* Ref. [6]).

3 Collider limits

3.1 Mono-jet limits

Weakly interacting dark matter particles can be detected at the LHC through their associated production with jets, electroweak bosons or heavy quarks. The search for such signatures together with large missing transverse energy (MET) has been performed at the LHC Run I and is one of the central goals of LHC Run II [3]. In the following we will focus on signatures with mono-jets and MET as presented in [21, 22]. Searches for electroweak gauge bosons with large MET are important in general, but provide weaker limits for the dark matter model we consider, see e.g. [25, 26].

To simulate the experimental signature for our model, we have generated events using FEYN-RULES 2.1 [27], MADGRAPH5_AMC@NLO [28] and PYTHIA 6 [29], including QCD processes with one and two jets in the hard scattering. We have used DELPHES [30] for the detector simulation and implemented the cuts employed in the ATLAS [21] and CMS [22] mono-jet

searches in an in-house program. With the observed and expected number of events provided by Refs. [21, 22] we are thus able to set exclusion limits at 95% confidence level (CL) on the different parameters of the model.

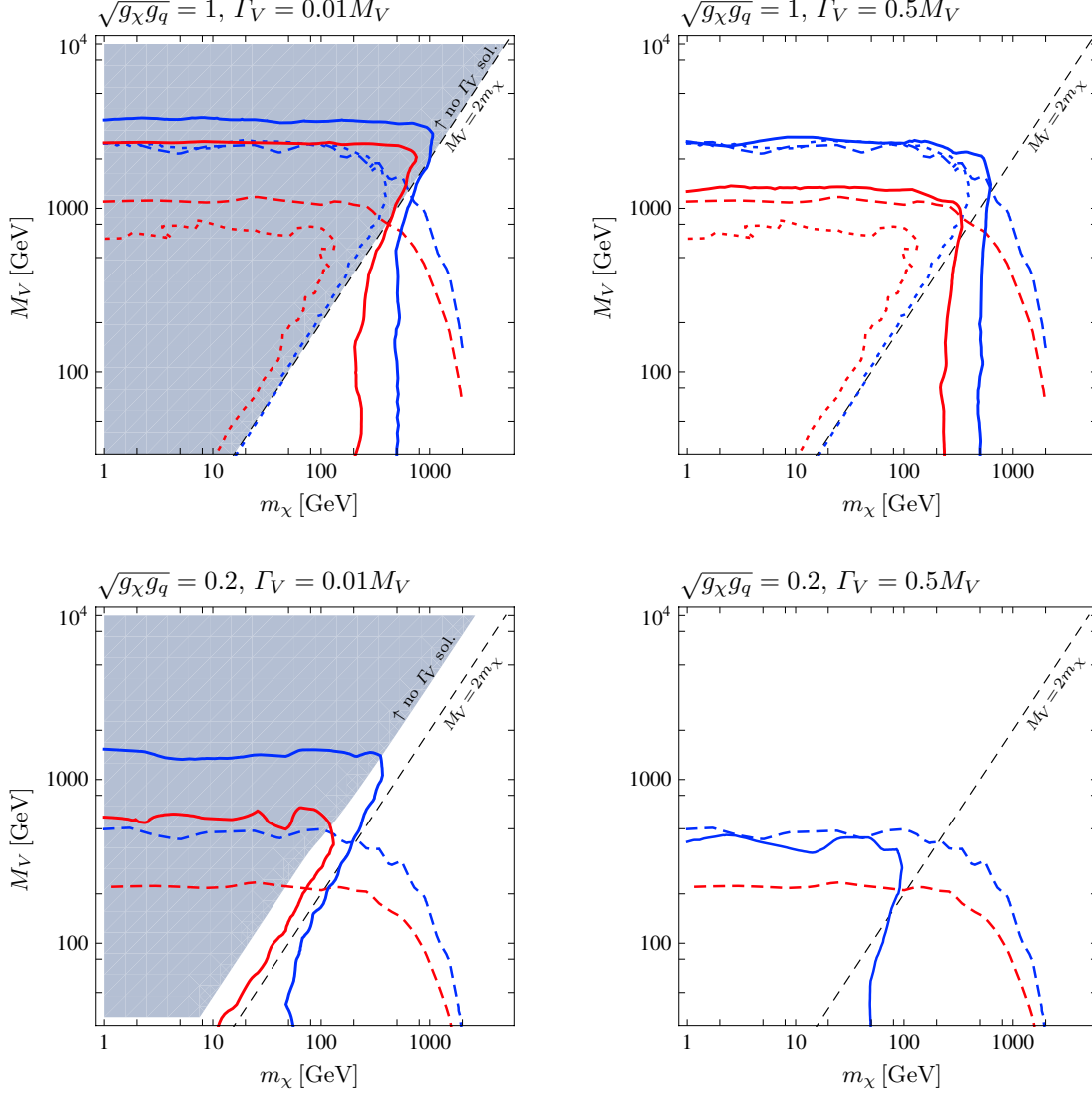


Figure 2: Lower exclusion limits in the m_χ - M_V plane at 95% CL for the ATLAS (blue lines) and CMS (red lines) mono-jet searches. The limits for the simplified model (solid lines), for the EFT (dashed lines) and for the EFT applying the Q -truncation (dotted lines) are shown. Four slices of the parameter space: $\sqrt{g_\chi g_q} = 1$, $\Gamma_V = 0.01 M_V$ (upper left panel), $\sqrt{g_\chi g_q} = 1$, $\Gamma_V = 0.5 M_V$ (upper right panel), $\sqrt{g_\chi g_q} = 0.2$, $\Gamma_V = 0.01 M_V$ (lower left panel) and $\sqrt{g_\chi g_q} = 0.2$, $\Gamma_V = 0.5 M_V$ (lower right panel) are displayed. The blue shaded region in the left panels represent the parameters space not allowing a consistent solution for the mediator width as a function of M_V , m_χ , $\sqrt{g_\chi g_q}$.

We have also studied our model in the EFT limit, where the interaction is described by a higher-dimensional operator of the form $(g_\chi g_q / M_V^2) \bar{\chi} \gamma_\mu \gamma^5 \chi \bar{q} \gamma^\mu \gamma^5 q$. As the EFT is valid only for energy scales below the mediator mass, it has been proposed to restrict the momentum transfer in the s -channel, $Q < M_V$, when calculating cross sections at the LHC [12].

In Fig. 2 we show exclusion limits on the dark matter and mediator masses, for scenarios with a small or a large mediator width, $\Gamma_V / M_V = 0.01$ and 0.5 , and small or large mediator couplings, $\sqrt{g_\chi g_q} = 0.2$ and 1 , respectively. Note that we consider $\Gamma_V / M = 0.5$ a rather extreme benchmark case, which however is commonly adopted in the literature. For even larger Γ_V / M

the narrow-width approximation to the cross section calculation may not be reliable, and the interpretation of the mediator as a resonance becomes doubtful. The results have been obtained for the ATLAS [21] and CMS [22] mono-jet searches interpreted in terms of the simplified model, the EFT, and the EFT with a truncation $Q < M_V$. Note that not all combinations of the parameters m_χ, M_V, Γ_V and $\sqrt{g_\chi g_q}$ are viable, as discussed in section 2: for a small width, $\Gamma_V/M_V = 0.01$, most of the region $M_V > 2m_\chi$ is theoretically inconsistent. On the other hand, for a large width $\Gamma_V/M_V = 0.5$ the whole parameter region is allowed.

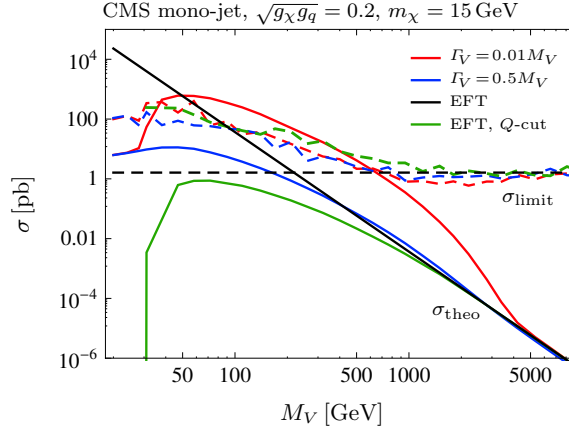


Figure 3: Theoretical prediction for the total production cross section (solid lines) and its observed upper limits (dashed lines) in the EFT limit with (green lines) and without (black lines) Q -truncation as well as in the simplified model with $\Gamma_V = 0.01M_V$ (red lines) and $\Gamma_V = 0.5M_V$ (blue lines). Example for $\sqrt{g_\chi g_q} = 0.2$ and $m_\chi = 15$ GeV for the CMS analysis.

We find large differences between the EFT and simplified model limits. For $M_V < 2m_\chi$ the EFT limit (without Q -truncation) extends to much larger values of m_χ and drastically overestimates the sensitivity in this region. By construction, this is not the case for the EFT limit employing the truncation on Q . Furthermore, also for $M_V > 2m_\chi$ we find significant differences. This is due to the fact that M_V lies in the range of accessible energies at the LHC. The cross section can be greatly enhanced due to contributions from on-shell mediators. This leads to a larger sensitivity in the simplified model than in the EFT and is most pronounced for a small mediator width. However, for small M_V – smaller than the minimal MET of approximately 150 GeV required in the search – the cross section in the simplified model decreases again and the sensitivity becomes weaker. This effect can be seen in the slice of parameter space with $\sqrt{g_\chi g_q} = 0.2$ and $\Gamma_V = 0.5M_V$ (lower right panel), where we cannot constrain the dark matter and mediator masses from the CMS analyses interpreted within the simplified model while within the EFT (without Q -truncation) a limit on M_V around 200 GeV is obtained.

To illustrate the origin of the differences we present the cross-section predictions together with the observed upper CMS limits for the simplified model, the EFT and the EFT with truncation in Fig. 3. The results are shown exemplarily for $\sqrt{g_\chi g_q} = 0.2$ and $m_\chi = 15$ GeV, and for small and large widths, $\Gamma_V/M_V = 0.01$ and 0.5 . The observed upper limits, which involve the observed number of events, the background expectation and the signal efficiencies, do not depend significantly on the mediator width, and are similar for the simplified model and the EFT with truncation. However, the cross section predictions from the simplified model and the EFT differ by orders of magnitude, in particular for small mediator widths. Furthermore, the simplified model cross section for $\sqrt{g_\chi g_q} = 0.2$ and $\Gamma_V/M_V = 0.5$ never exceeds the cross section limit, so that no constraint on the dark matter and mediator masses can be derived. Note that the slopes of the cross section limits and the cross section predictions are quite similar, so that small changes in the observed number of events, or small statistical fluctuations in the estimate

of the efficiencies and cross sections, may have a visible impact on the limits.

We conclude that for our dark matter model, the EFT interpretation of the experimental LHC searches is only reliable if the mediator mass is larger than the accessible LHC partonic energies. However, as the current LHC limit on the suppression scale $M_* = M_V/\sqrt{g_\chi g_q}$ is of $\mathcal{O}(1 \text{ TeV})$, an EFT interpretation would require extremely large couplings. On the other hand, the EFT limit with a truncation on Q results in overly conservative limits which do not fully exploit the potential of the LHC searches. We will thus use the limits obtained in the simplified model in the compilation of bounds presented in section 5.

3.2 Di-jet limits

Limits on our simplified model can also be derived from searches for the mediator particle in di-jet signatures. A detailed and comprehensive study of di-jet constraints has been presented recently in Ref. [10], including results from UA2 [31], the Tevatron [32], ATLAS [33, 34] and CMS [35]. These searches can set bounds on a broad range of masses and are complementary to the signatures we have studied in this paper. We will include the di-jet limits in the final discussion of the bounds on the model parameter space presented in section 5.

4 Astrophysical and cosmological constraints

Models for dark matter are constrained by the relic density, indirect and direct searches. We have evaluated the relic density and the most recent IceCube limits on dark matter annihilation in the Sun [23] within our simplified model for Majorana dark matter, as discussed in detail below. We also briefly comment on direct dark matter searches, which provide further complementary constraints on our model.

4.1 Relic density

We have calculated the dark matter relic density for each point of the model parameter space using FEYNRULES 2.1 [27], CALCHEP [36] and MICROMEGAS 4 [37]. The calculation includes possible resonant effects, which are not taken into account when expanding in the dark matter velocity [38]. We have however checked that the results obtained from the exact calculation within the simplified model match those obtained in the EFT limit for $M_V \gg m_\chi$. To that end, we have calculated the annihilation cross section into quarks [39, 40] for the case of Majorana dark matter,

$$\sigma_{qq} = \frac{g_q^2 g_\chi^2}{4\pi} \frac{1}{s M_V^4 (M_V^2 - s)^2} \frac{\beta_q}{\beta_\chi} \left(4M_V^4 [28m_q^2 m_\chi^2 - 4s(m_\chi^2 + m_q^2) + s^2] \right. \\ \left. - 96M_V^2 m_\chi^2 m_q^2 s + 48m_\chi^2 m_q^2 s^2 \right), \quad (3)$$

where $\beta_{q,\chi} = \sqrt{1 - 4m_{q,\chi}^2/s}$ and s is the center-of-mass energy. Note that this annihilation cross section is helicity suppressed [41, 42], and thus the main annihilation channels will be into top and bottom quarks.

In Fig. 6 (grey band) we show the parameter values of our model for which the relic density from thermal freeze-out agrees with the one measured by the Planck Collaboration [43], $\Omega_{\text{DM}} h^2 = 0.1199$, within $\pm 10\%$. Assuming a standard cosmological history parameter points above this line can be considered excluded in the framework of our simplified model. Points below this line could be allowed by either requiring an additional component of dark matter or an additional (non-thermal) production mechanism. In this paper we assume 100% of the (local)

dark matter to be the considered WIMP candidate and hence do not rescale the limits from IceCube and LUX for points below the grey band. Note that in an extension of our simplified model co-annihilations or additional resonances may exist that could further weaken the relic density constraint while providing a similar phenomenology at the LHC and IceCube.

Finally, we mention that the unitarity of the S -matrix imposes constraints on the masses and couplings in the dark matter model [10, 44]. However, performing a definite analysis of unitarity constraints would require us to extend the simplified model framework, which is beyond the scope of this work.

4.2 Limits from IceCube

If dark matter particles scatter in heavy astrophysical objects such as the Sun, they can lose enough energy to become gravitationally trapped inside the object. With the accumulation of dark matter, the annihilation rate can become large enough to lead to an equilibrium between dark matter capture and annihilation.

The evolution of the number of dark matter particles in the Sun, N , can be described by the Riccati differential equation [45]

$$\dot{N} = C_{\odot} - C_A N^2 - C_E N, \quad (4)$$

where \dot{N} denotes the time derivative of N , C_{\odot} is the capture rate of dark matter particles in the Sun, $C_A N^2 = 2\Gamma_A$ is twice the dark matter annihilation rate and $C_E N$ is the evaporation rate, *i.e.* the rate at which particles escape the Sun due to hard elastic scattering. For dark matter particles with masses $m_{\chi} \gtrsim 10 \text{ GeV}$, the evaporation term can be neglected [46], allowing for a simple solution of Eq. (4):

$$C_A N^2 = C_{\odot} \tanh^2 \left(\sqrt{C_{\odot} C_A} t \right). \quad (5)$$

For large times, $\sqrt{C_{\odot} C_A} t \gg 1$, the tanh-term in Eq. (5) approaches one, and WIMP annihilation and capture are in equilibrium, *i.e.* $C_{\odot} = 2\Gamma_A = C_A N^2$. This implies $\dot{N} = 0$. Hence in equilibrium the annihilation rate does not depend on the annihilation cross section, but only on the capture rate, which in turn is determined by the elastic WIMP scattering cross section. We shall analyze the equilibrium condition within our model in more detail in Sec. 4.2.3.

Through a measurement of the neutrino flux, neutrino telescopes are sensitive to the WIMP annihilation rate. We consider data from the IceCube Neutrino Observatory [47, 23] taken during 317 days in the years 2011 and 2012. No significant excess over background has been observed and these measurements can thus be used to set limits on possible dark matter signals.

The search has been interpreted in terms of limits on the spin-dependent WIMP-proton scattering cross section. The WIMP-nucleon scattering cross section in our model is

$$\begin{aligned} \sigma_{\text{SD}}^{(N)} &= \frac{12\mu_{N\chi}^2 g_{\chi}^2}{\pi M_V^4} \left(\sum_{q=u,d,s} g_q \Delta_q^{(N)} \right)^2 \\ &\simeq 1.8 \times 10^{-40} \text{ cm}^2 \left(\frac{\mu_{N\chi}}{1 \text{ GeV}} \right)^2 \left(\frac{g_{\chi} g_q}{1} \right)^2 \left(\frac{1 \text{ TeV}}{M_V} \right)^4, \end{aligned} \quad (6)$$

where $\mu_{N\chi} = m_{\chi} m_N / (m_{\chi} + m_N)$ is the reduced WIMP-nucleon mass and $N = p$ for WIMP-proton scattering.² In the second line of Eq. (6) we have used the fact that g_q is universal and included the numerical values for the nucleon form factors $\Delta_u^{(p)} = \Delta_d^{(n)} = 0.85$, $\Delta_u^{(n)} =$

²The scattering cross section for Majorana fermion dark matter given in Eq. (6) is larger than the one for Dirac fermion dark matter by a factor of four (see *e.g.* Ref. [48]). This is in contradiction with the result quoted in Ref. [49], which is a factor of eight smaller than our result.

$\Delta_d^{(p)} = -0.42$ and $\Delta_s^{(p)} = \Delta_s^{(n)} = -0.08$ [50]. Considering universal couplings and neglecting the small mass difference between the proton and the neutron, the WIMP-neutron scattering cross section probed in direct detection experiments (see section 4.3) is equal to the WIMP-proton cross section.

The dark matter interpretation of the IceCube searches initially relied on two scenarios: annihilation into $b\bar{b}$ and W^+W^- [47]. Recently, an improved interpretation [23] has been performed which includes more scenarios, in particular annihilation into $t\bar{t}$. In the model considered here, annihilation into $t\bar{t}$, $b\bar{b}$ and VV is dominant (*cf.* Fig. 6). Therefore, in Sec. 4.2.1 we will first estimate the limit on the spin-dependent WIMP-proton scattering cross section for annihilation into $t\bar{t}$ based on the limits for the annihilation into W^+W^- and $b\bar{b}$. The excellent agreement between our estimate of the $t\bar{t}$ limits and the results presented in Ref. [23] is considered as evidence for the accuracy of the conversion method. We then apply the same method to estimate limits on the annihilation into VV in Sec. 4.2.2. For the exclusion limits on the parameter space of our model we conservatively take into account only the most constraining channel and compute the model rejection factor, μ , via

$$\mu(m_\chi, M_V) = \sigma_{\text{SD}}^{(p)}(m_\chi, M_V) \times \max \left(\frac{R_{t\bar{t}}(m_\chi, M_V)}{\sigma_{t\bar{t}}^{\text{UL}}(m_\chi)}, \frac{R_{b\bar{b}}(m_\chi, M_V)}{\sigma_{b\bar{b}}^{\text{UL}}(m_\chi)}, \frac{R_{VV}(m_\chi, M_V)}{\sigma_{VV}^{\text{UL}}(m_\chi, M_V)} \right), \quad (7)$$

where R_i is the contribution of the channel i to the annihilation cross section and σ_i^{UL} is the corresponding upper limit on the spin-dependent WIMP-proton scattering cross section. Note that we display the dependence of the various factors on the dark matter and mediator masses, but not the dependence on the couplings g_q, g_χ . A point in parameter space is excluded if $\mu \geq 1$.

4.2.1 Limit on σ_{SD} for annihilation into $t\bar{t}$

In this subsection we will derive a limit on the spin-dependent WIMP-proton scattering cross section for dark matter annihilating to 100% into $t\bar{t}$. Our procedure uses the limits of capturing rates Γ_A for annihilation into W^+W^- and $b\bar{b}$ as input. As WIMPs are practically at rest inside the Sun, the W bosons (or b quarks) that are produced directly in WIMP annihilation have a well-defined energy given by the WIMP mass m_χ . Therefore we can interpret the limits on Γ_A as limits on the annihilation rate of the W -(or b)-pairs with the energy $E^{W/b} = m_\chi$, regardless of the actual annihilation process.³ We exploit this fact and consider the energy spectrum of the W bosons and b quarks arising from the decay of the top quarks from WIMP annihilation into $t\bar{t}$. Since the interaction time of the top quark in the Sun is much larger than its lifetime, no energy loss is expected before it decays into an on-shell W -boson and b -quark. As a next step we calculate the probability distributions $P(E_i|E_t)$ of the energy of a final state particle i for a given top energy – and hence WIMP mass – by simulating the annihilation process $\chi\chi \rightarrow t\bar{t} \rightarrow W^+W^-b\bar{b}$ with MADGRAPH5_AMC@NLO. The probability distributions are normalized to one. Based on these distributions we can calculate the resulting limit on $\Gamma_A^{t\bar{t}}$ by a weighted average of the limits for each relevant final state $x = W^+, W^-, b, \bar{b}$:

$$\frac{1}{\Gamma_A^{t\bar{t}}(E_t)} = \int_0^\infty dE_W \frac{P(E_W|E_t)}{\Gamma_A^{W^+W^-}(E_W)} + \int_0^\infty dE_b \frac{P(E_b|E_t)}{\Gamma_A^{b\bar{b}}(E_b)}. \quad (8)$$

In order to evaluate $\Gamma_A^{W^+W^-/b\bar{b}}$ for arbitrary values of the energy we interpolate the limits linearly in $E^{W/b}$ between the values given in Ref. [23] on a double logarithmic scale. Note that

³Note that this is only true for the limit on Γ_A , but not for the limit on σ_{SD} because σ_{SD} depends explicitly on m_χ through the capture efficiencies. Furthermore, the limit on Γ_A is independent of the correlation between the two W bosons (or b quarks) of one annihilation. The fraction of events where multiple neutrinos arising from W bosons (or b quarks) of the same annihilation simultaneously interact in the detector can safely be neglected.

the contribution from the b quarks in Eq. (8) is sub-leading. The correction is below 10% (for large WIMP masses and decreases to below 1% towards small masses).

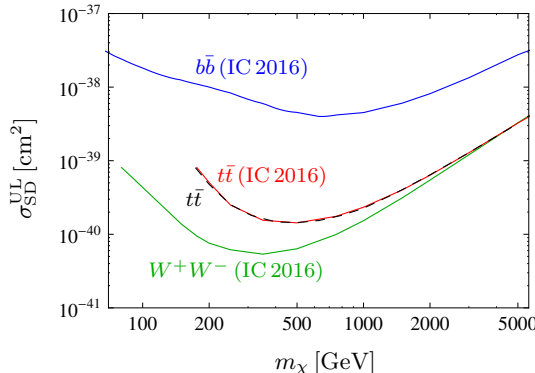


Figure 4: 90% CL upper limits on the spin-dependent WIMP-proton scattering cross section, σ_{SD}^{UL} , for 100% annihilation into $t\bar{t}$ (red solid line), $b\bar{b}$ (blue dotted line) and W^+W^- (green dashed line) from the IceCube Neutrino Observatory [23]. The black dashed line shows the $t\bar{t}$ limit we derived from the $b\bar{b}$ and W^+W^- data according to the method described in Sec. 4.2.1.

We converted the limits on the spin-dependent WIMP-proton scattering cross section given in Ref. [23] into limits on the annihilation rate (and vice versa) by

$$\Gamma_A^{UL}(m_\chi) = \frac{1}{2} K_{SD}(m_\chi) \sigma_{SD}^{UL}(m_\chi), \quad (9)$$

where K_{SD} is the (channel independent) capture efficiency for the spin-dependent part of the scattering. We take K_{SD} from Ref. [47] where it was derived following the method of Ref. [51] adopting the Standard Solar Model BS05(OP) [52] as implemented in DARKSUSY [53].

The result is presented in Fig. 4, where we also show the limit on 100% annihilation into W^+W^- , $b\bar{b}$ and $t\bar{t}$ from Ref. [23]. The good agreement of our cross section limits for $t\bar{t}$ with Ref. [23] demonstrates the validity of our calculation. In addition, as a consistency check of our procedure, we have converted the limit on the annihilation rate into a limit on the resulting muon flux in the detector, Φ_μ^{UL} , using the conversion functions provided in Ref. [51]. As expected, we found that Φ_μ^{UL} from the annihilation into $t\bar{t}$ is always in between the limits obtained for annihilation into W^+W^- and $b\bar{b}$ as presented in Ref. [23].

4.2.2 Limit on σ_{SD} for annihilation into VV

In this subsection we will derive limits on the spin-dependent WIMP-proton scattering cross section for dark matter annihilating to 100% into mediator pairs VV with the method described in Sec. 4.2.2. Annihilation into VV takes place only for $M_V < m_\chi$, where the mediator decays solely into quarks. As we consider a universal coupling to all quarks, the corresponding branching ratios are simply determined by the accessible phase space. Here we only take into account neutrinos arising from the decay of the mediator into bottom and top quarks. In order to justify this choice we computed the differential neutrino spectra dn_ν/dE_ν for annihilation into all quark flavors with WIMPSIM 3 [54].⁴ As expected, the neutrino fluxes spectra for light flavor quarks d, u, s are much softer than for bottom and top quarks and can be safely neglected for the derivation of the limits. The neutrino flux for annihilation into charm quarks is weaker than

⁴The program package WIMPSIM is linked to PYTHIA 6 [29] for the simulation of dark matter annihilation in the Sun, NUSIGMA [55] for the simulation of neutrino-nucleon interactions and to DARKSUSY [53] for the implementation of the Sun's density profile. We take the neutrino oscillation parameters from Ref. [56].

that for b -quarks by a factor of 3 to 10 (and much weaker than for top quarks) in the relevant energy range and is hence subdominant. We simulate the annihilation process $\chi\chi \rightarrow VV$ and the subsequent decays $V \rightarrow q\bar{q}$ with MADGRAPH5_AMC@NLO and determine the probability distributions $P(E_q|E_V)$ of the energy of a final state quark $q = b, t$, which are hence normalized to $2 \times \text{BR}(V \rightarrow q\bar{q})$. We calculate the resulting limit on Γ_A^{VV} analogous to Eq. (8) through:

$$\frac{1}{\Gamma_A^{VV}(E_V)} = \int_0^\infty dE_t \frac{P(E_t|E_V)}{\Gamma_A^{tt}(E_t)} + \int_0^\infty dE_b \frac{P(E_b|E_V)}{\Gamma_A^{bb}(E_b)}. \quad (10)$$

As the resulting limit depends on the WIMP mass and the mediator mass we scan the corresponding two-dimensional grid. In Fig. 5 we present the limits on Γ_A (left panel) and σ_{SD}^{VV} (right panel). The limits are considerably weaker than for annihilation into a pair of tops. As the limits depend both on m_χ and M_V we show two slices in the parameter space $M_V/m_\chi = 0.75$ and $M_V/m_\chi = 0.35$, respectively. The main difference between these two slices is due to the opening of the mediator decay into top quarks for $M_V > 2m_t$, which greatly enhances the sensitivity.

The resulting IceCube limits on the model parameter space considering the annihilation channels $b\bar{b}$, $t\bar{t}$ and VV are shown in Fig. 6. The sensitivity to annihilation into VV is significantly weaker than for $t\bar{t}$ and – below the $t\bar{t}$ threshold – for $b\bar{b}$ final states. This causes a drop in the limit on M_V for regions where annihilation into VV is dominant (light grey areas).

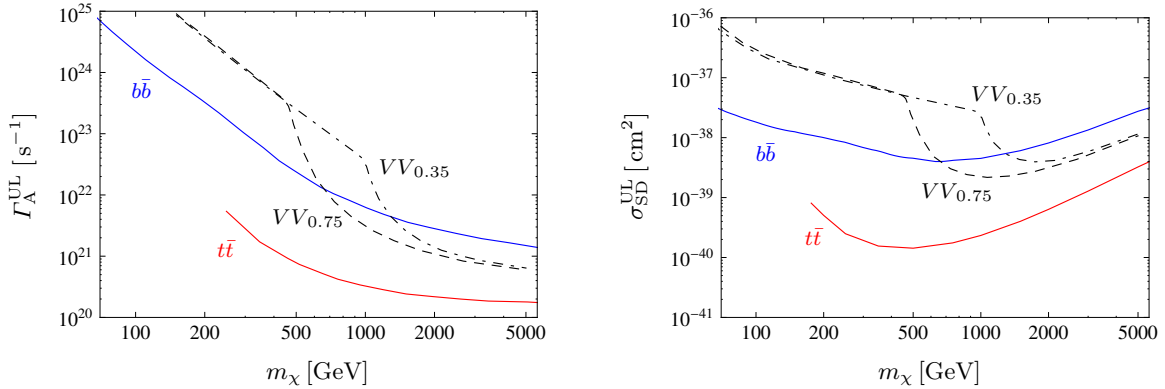


Figure 5: 90% CL upper limits on the annihilation rate Γ_A and the spin-dependent WIMP-proton scattering cross section σ_{SD} for 100% annihilation into VV (black lines) derived from a reinterpretation of the data from the IceCube Neutrino Observatory [23]. We show two slices regarding the mediator mass, $M_V/m_\chi = 0.75$ (dashed line) and $M_V/m_\chi = 0.35$ (dot-dashed line). For comparison we also show the limits for 100% annihilation into $b\bar{b}$ (blue solid line) and W^+W^- (red solid line) taken from Ref. [23].

4.2.3 Equilibrium condition for capturing and annihilation in the Sun

As discussed at the beginning of Sec. 4.2, for large times, $\sqrt{C_\odot C_A} t \gg 1$, dark matter matter annihilation and capture in the Sun are in equilibrium, and the limits on the annihilation rate can directly be translated into limits on the elastic WIMP-nucleon scattering. Assuming that the Sun has been collecting dark matter during its entire lifetime, $t = t_\odot \simeq 1.5 \times 10^{17} \text{ s}$, the equilibrium condition can approximately be expressed by [45]

$$\sqrt{C_\odot C_A} t_\odot \simeq 330 \left(\frac{C_\odot}{\text{s}^{-1}} \right)^{1/2} \left(\frac{\langle \sigma_A v \rangle}{\text{cm}^3 \text{ s}^{-1}} \right)^{1/2} \left(\frac{m_\chi}{10 \text{ GeV}} \right)^{3/4} \gg 1. \quad (11)$$

In practice $\sqrt{C_\odot C_A} t_\odot \gtrsim 3$ is already enough to obtain an error of less than a percent on C_\odot . In order to estimate $\sqrt{C_\odot C_A} t_\odot$ for our model, we compute $\langle \sigma_A v \rangle$ with MICROMEGAS. The

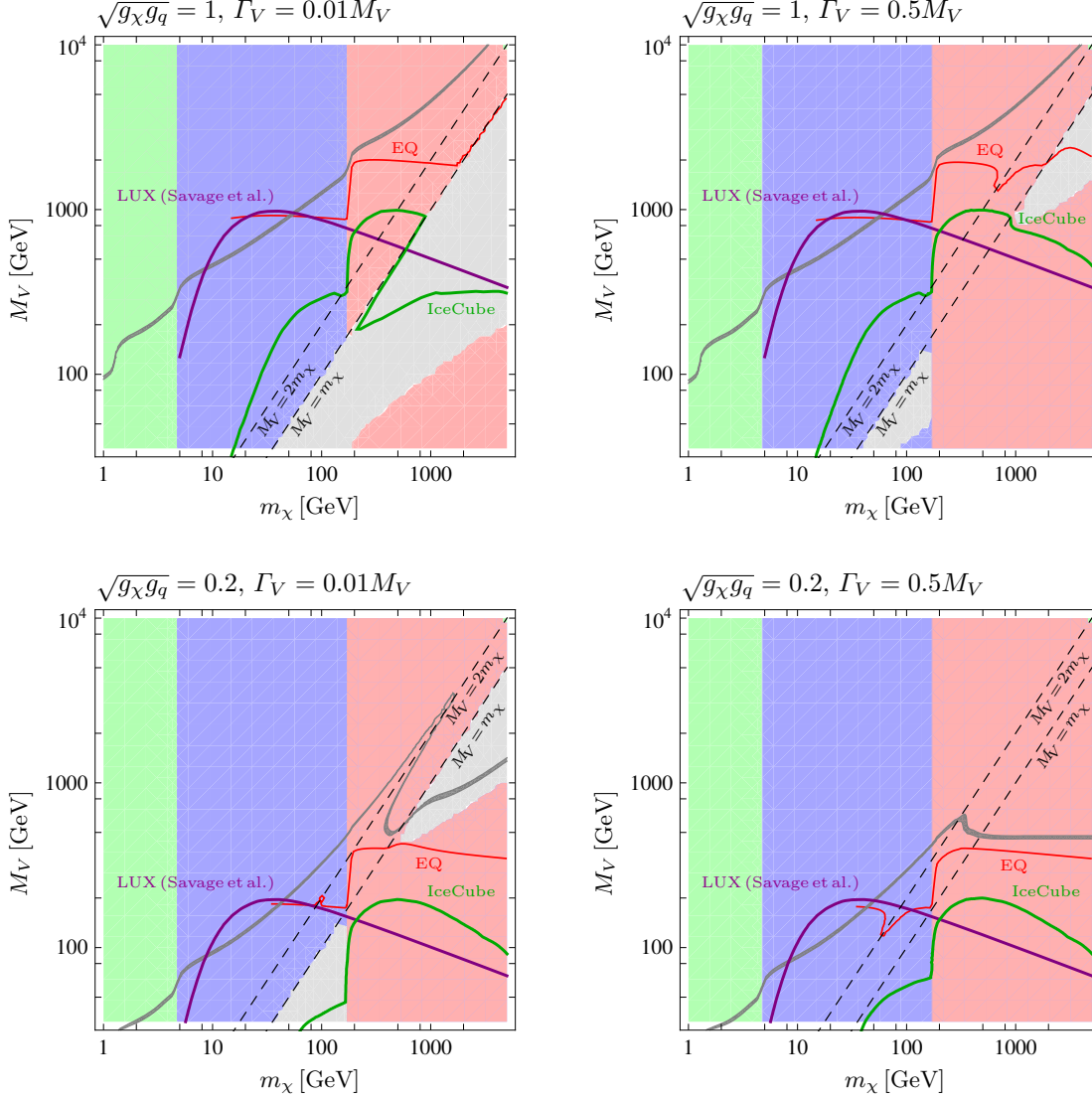


Figure 6: Astrophysical and cosmological quantities in the m_χ - M_V plane in four slices of the considered parameter space: $\sqrt{g_\chi g_q} = 1$, $\Gamma_V = 0.01 M_V$ (upper left panel), $\sqrt{g_\chi g_q} = 1$, $\Gamma_V = 0.5 M_V$ (upper right panel), $\sqrt{g_\chi g_q} = 0.2$, $\Gamma_V = 0.01 M_V$ (lower left panel) and $\sqrt{g_\chi g_q} = 0.2$, $\Gamma_V = 0.5 M_V$ (lower right panel). The shaded regions denote the dominant annihilation channel, in red, blue, green and grey we denote dominant annihilation into $t\bar{t}$, $b\bar{b}$, light flavor quarks and two mediators, respectively. The 90% CL lower exclusion limits from the IceCube Neutrino Observatory (green line) and from LUX derived from the limits presented in Ref. [49] (purple line) are also displayed. The dark grey shaded band denotes the region where the relic density matches the dark matter density within $\pm 10\%$. In the region below the red thin line the equilibrium condition is fulfilled, *i.e.* $\sqrt{C_\odot C_A} t_\odot > 3$.

capture rate, C_\odot , can be deduced from the WIMP-nucleon scattering cross section using the capture efficiency (see Sec. 4.2.1)

$$C_\odot = K_{SD}(m_\chi) \sigma_{SD}. \quad (12)$$

In Fig. 6 we show the contours $\sqrt{C_\odot C_A} t_\odot = 3$ (labeled “EQ”) in the m_χ - M_V plane. Below this line the equilibrium condition is fulfilled and the interpretation of the IceCube measurement in terms of the elastic scattering cross section is justified. A similar conclusion was put forward for the limits set in Ref. [4], where $\langle \sigma_A v \rangle$ was computed within the EFT. However, the fact that the equilibrium condition holds in the EFT limit does not imply that it should hold in the simplified model description, as the thermally averaged cross section, $\langle \sigma_A v \rangle$, can be smaller in

the latter case.

4.3 Limits from direct detection

Although providing much stronger limits on the spin-independent WIMP-nucleon scattering cross section, direct detection experiments are also capable of imposing limits on spin-dependent scattering. In the relevant part of the parameter space the strongest constraints are set by the LUX experiment [57]. As an up-to-date dedicated analysis for spin-dependent scattering has not been provided by the LUX Collaboration, several authors have reinterpreted the LUX limits accordingly [7, 49, 10].

We will use the limits on the spin-dependent WIMP-neutron scattering cross section presented in Ref. [49]. They are very similar to those presented in Ref. [7]. Since Xenon, the target material of LUX, has neutron-odd isotopes, limits on spin-dependent WIMP-proton scattering are considerably weaker and are thus not taken into account. The results are shown in Fig. 6 (purple curve).

5 Results and Discussion

In this section we finally summarize the constraints on our model from indirect, direct and collider searches. Fig. 7 presents limits on the dark matter and mediator masses for four different choices of the coupling strength, $\sqrt{g_\chi g_q}$, and the mediator width, Γ_V . As discussed in Sec. 2, not all combinations of the parameters m_χ, M_V, Γ_V and $\sqrt{g_\chi g_q}$ are viable within our model. For small width, a large range of the parameter space, marked in shaded blue in the left panels of Fig. 7, is not allowed. For a large width, $\Gamma_V = 0.5 M_V$, on the other hand, the whole parameter region is allowed.

The model provides the correct dark matter relic density only for the parameter region within the thin grey band. The shaded grey area in Fig. 7 indicates the parameter region leading to an overproduction of dark matter within the model. Note, however, that the relic density constraint can be softened significantly if we assume an extended particle spectrum that leads to co-annihilation effects (which can give access to the region above the thermal relic-band) or to additional – non-thermal – contributions to the dark matter production (which can give access to the region below the thermal relic-band).

The limits from the ATLAS and CMS mono-jet searches, obtained within the simplified model, are particularly relevant for small m_χ . The ATLAS mono-jet analysis (blue solid curve) is the most constraining search for $M_V > 2m_\chi$ in the whole parameter space considered. In particular, this search constrains most strongly the parameter space where the relic density from thermal freeze-out agrees with the measured dark matter density, *cf.* the dark grey band that represents the parameter region with $\Omega_{\text{th}} h^2 = 0.1199 \pm 0.012$. The LHC limits depend upon the width of the mediator. This dependence is particularly pronounced for $\sqrt{g_\chi g_q} = 0.2$, where LHC searches probe mediator masses $M_V \lesssim 1 \text{ TeV}$. Note that this mass range is of the order of the typical scattering energies of mono-jet searches with large MET, so that an EFT description would not be reliable. The sensitivity of the LHC searches is higher for smaller width as the cross section is enhanced through on-shell mediator production.

As discussed in Sec. 3.2 we also show the limits from di-jet searches as obtained in Ref. [10]. These constraints are particularly important for large mediator width (right panels), because a larger width requires a larger mediator-quark coupling g_q , and thus a larger cross section.

The direct and indirect dark matter searches by the LUX and IceCube experiments, respectively, are particularly relevant for intermediate and large dark matter masses. The IceCube limits, specifically, show a maximal sensitivity for dark matter masses around 200–1000 GeV. This results from two effects: As the sensitivity for annihilation into $b\bar{b}$ is significantly lower

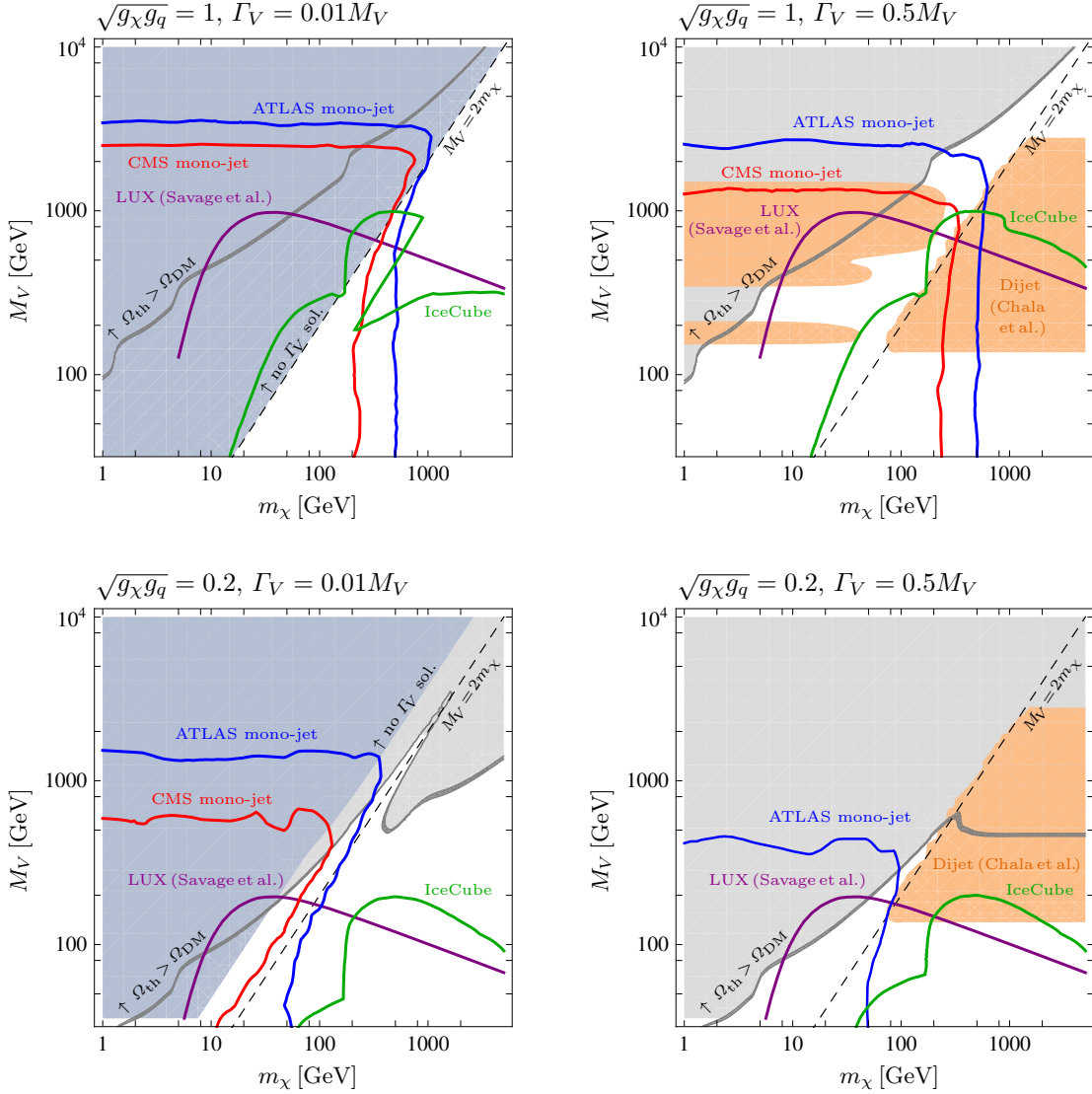


Figure 7: Summary of the exclusion limits in the m_χ - M_V plane in four slices of the considered parameter space: $\sqrt{g_\chi g_q} = 1$, $\Gamma_V = 0.01 M_V$ (upper left panel), $\sqrt{g_\chi g_q} = 1$, $\Gamma_V = 0.5 M_V$ (upper right panel), $\sqrt{g_\chi g_q} = 0.2$, $\Gamma_V = 0.01 M_V$ (lower left panel) and $\sqrt{g_\chi g_q} = 0.2$, $\Gamma_V = 0.5 M_V$ (lower right panel). We show the 95% CL lower exclusion limits from mono-jet searches at ATLAS (blue lines) and CMS (red lines) (both in the simplified model interpretation) as well as limits from searches for resonances in di-jet signatures taken from Ref. [10] (orange shaded regions are excluded). Furthermore, we show the 90% CL lower exclusion limits from the IceCube Neutrino Observatory (green line) and from LUX derived from the limits presented in Ref. [49] (purple line). The dark grey shaded band denotes the region where the relic density matches the dark matter density within $\pm 10\%$. In the light-grey shaded region above it, the dark matter is over-produced. The blue shaded region in the left panels do not allow for a consistent solution for the mediator width as a function of $M_V, m_\chi, \sqrt{g_\chi g_q}$ within the model.

than for $t\bar{t}$ (*cf.* Fig. 4) there is a significant strengthening of the IceCube limits around the top threshold. For very large m_χ , on the other hand, the capture efficiencies and thus the cross section limits decrease and the IceCube search loses sensitivity. Furthermore, for $M_V < m_\chi/2$, the annihilation into a pair of mediators is allowed (via a t -channel χ), which again provides a lower model rejection than $t\bar{t}$. Hence, the limit depends strongly on the relative importance of annihilation into $t\bar{t}$ and VV . For $m_\chi > M_V$ and $\sqrt{g_\chi g_q} = 1$, the limit is considerably weaker for a small mediator width, as a smaller width requires a smaller g_q and hence a larger g_χ (note that the cross section for annihilation into mediators scales like g_χ^4).

6 Conclusion

The complementarity of direct, indirect and collider searches for dark matter can be exploited in the framework of simplified models, where dark matter and its experimental signatures are described with a minimal amount of new particles, interactions and model parameters. We have considered a simplified model with a Majorana fermion dark matter particle and an axial-vector mediator with universal couplings to SM quarks. Such a model leads to spin-dependent interactions and can thus be probed by IceCube in the search for neutrinos from dark matter annihilation in the Sun.

We have focused on a re-interpretation of IceCube limits on the dark matter annihilation rate within our model, and have obtained substantial constraints on the dark matter and mediator masses. Furthermore, we have derived new constraints on our model from recent LHC mono-jet searches, and have analyzed in some detail the differences between interpretations of LHC searches within simplified models and effective field theories.

We find that the limits from the ATLAS and CMS mono-jet searches are particularly relevant for small dark matter masses. They exclude mediator masses $M_V \lesssim 1$ TeV, depending in detail on the size of the couplings and the mediator width. The indirect searches for dark matter annihilation in the Sun by IceCube probe intermediate and large dark matter masses and show a maximal sensitivity for masses $m_\chi \simeq 200\text{--}1000$ GeV. In this region, the dark matter capture efficiencies in the Sun are still sizeable, and dark matter annihilation is predominantly into top quarks, leading to more highly energetic neutrinos and thus a higher neutrino detection efficiency with IceCube.

We have also computed the relic density within our model, and have combined the LHC mono-jet and IceCube limits with constraints from direct detection and the collider search for di-jet resonances. We have found a striking complementarity of the different experimental approaches, which probe particular and often distinct regions of the model parameter space. Thus, the combination of future collider, indirect and direct searches for dark matter will allow a comprehensive test of minimal dark matter models.

Acknowledgments

We would like to thank Chiara Arina, Pavel Gretskov, Carlos de los Heros, Kerstin Hoepfner, Alexander Knochel, Manfred Krauss, Lennart Oymanns, Mohamed Rameez, Carsten Rott, Pat Scott and Jory Sonnenveld for helpful discussions. We acknowledge support by the German Research Foundation DFG through the research unit “New physics at the LHC”, the Helmholtz Alliance for Astroparticle Physics and the German Federal Ministry of Education and Research BMBF.

References

- [1] J. Abdallah, A. Ashkenazi, A. Boveia, G. Busoni, A. De Simone, *et al.*, *Simplified Models for Dark Matter and Missing Energy Searches at the LHC*. [arXiv:1409.2893](#) [[hep-ph](#)].
- [2] S. A. Malik *et al.*, *Interplay and Characterization of Dark Matter Searches at Colliders and in Direct Detection Experiments*. [Phys. Dark Univ. **9-10** \(2015\) 51–58](#), [arXiv:1409.4075](#) [[hep-ex](#)].
- [3] D. Abercrombie, N. Akchurin, E. Akilli, J. A. Maestre, B. Allen, *et al.*, *Dark Matter Benchmark Models for Early LHC Run-2 Searches: Report of the ATLAS/CMS Dark Matter Forum*. [arXiv:1507.00966](#) [[hep-ex](#)].

- [4] J. Blumenthal, P. Gretskev, M. Krämer, and C. Wiebusch, *Effective field theory interpretation of searches for dark matter annihilation in the Sun with the IceCube Neutrino Observatory*. *Phys.Rev.* **D91** (2015) no. 3, 035002, [arXiv:1411.5917 \[astro-ph.HE\]](#).
- [5] R. Catena, *Dark matter signals at neutrino telescopes in effective theories*. *JCAP* **1504** (2015) no. 04, 052, [arXiv:1503.04109 \[hep-ph\]](#).
- [6] O. Buchmueller, M. J. Dolan, and C. McCabe, *Beyond Effective Field Theory for Dark Matter Searches at the LHC*. *JHEP* **1401** (2014) 025, [arXiv:1308.6799 \[hep-ph\]](#).
- [7] O. Buchmueller, M. J. Dolan, S. A. Malik, and C. McCabe, *Characterising dark matter searches at colliders and direct detection experiments: Vector mediators*. *JHEP* **1501** (2015) 037, [arXiv:1407.8257 \[hep-ph\]](#).
- [8] O. Lebedev and Y. Mambrini, *Axial dark matter: The case for an invisible Z'* . *Phys. Lett.* **B734** (2014) 350–353, [arXiv:1403.4837 \[hep-ph\]](#).
- [9] A. Alves, A. Berlin, S. Profumo, and F. S. Queiroz, *Dark Matter Complementarity and the Z' Portal*. [arXiv:1501.03490 \[hep-ph\]](#).
- [10] M. Chala, F. Kahlhoefer, M. McCullough, G. Nardini, and K. Schmidt-Hoberg, *Constraining Dark Sectors with Monojets and Dijets*. *JHEP* **07** (2015) 089, [arXiv:1503.05916 \[hep-ph\]](#).
- [11] G. Busoni, A. De Simone, E. Morgante, and A. Riotto, *On the Validity of the Effective Field Theory for Dark Matter Searches at the LHC*. *Phys.Lett.* **B728** (2014) 412–421, [arXiv:1307.2253 \[hep-ph\]](#).
- [12] G. Busoni, A. De Simone, J. Gramling, E. Morgante, and A. Riotto, *On the Validity of the Effective Field Theory for Dark Matter Searches at the LHC, Part II: Complete Analysis for the s -channel*. *JCAP* **1406** (2014) 060, [arXiv:1402.1275 \[hep-ph\]](#).
- [13] Y. Bai, P. J. Fox, and R. Harnik, *The Tevatron at the Frontier of Dark Matter Direct Detection*. *JHEP* **12** (2010) 048, [arXiv:1005.3797 \[hep-ph\]](#).
- [14] P. J. Fox, R. Harnik, J. Kopp, and Y. Tsai, *Missing Energy Signatures of Dark Matter at the LHC*. *Phys. Rev.* **D85** (2012) 056011, [arXiv:1109.4398 \[hep-ph\]](#).
- [15] P. J. Fox, R. Harnik, J. Kopp, and Y. Tsai, *LEP Shines Light on Dark Matter*. *Phys. Rev.* **D84** (2011) 014028, [arXiv:1103.0240 \[hep-ph\]](#).
- [16] P. J. Fox and C. Williams, *Next-to-Leading Order Predictions for Dark Matter Production at Hadron Colliders*. *Phys. Rev.* **D87** (2013) no. 5, 054030, [arXiv:1211.6390 \[hep-ph\]](#).
- [17] J. Goodman and W. Shepherd, *LHC Bounds on UV-Complete Models of Dark Matter*. [arXiv:1111.2359 \[hep-ph\]](#).
- [18] G. Busoni, A. De Simone, T. Jacques, E. Morgante, and A. Riotto, *On the Validity of the Effective Field Theory for Dark Matter Searches at the LHC Part III: Analysis for the t -channel*. *JCAP* **1409** (2014) 022, [arXiv:1405.3101 \[hep-ph\]](#).
- [19] M. R. Buckley, D. Feld, and D. Goncalves, *Scalar Simplified Models for Dark Matter*. *Phys. Rev.* **D91** (2015) 015017, [arXiv:1410.6497 \[hep-ph\]](#).

- [20] P. Harris, V. V. Khoze, M. Spannowsky, and C. Williams, *Constraining Dark Sectors at Colliders: Beyond the Effective Theory Approach*. [Phys. Rev. **D91** \(2015\) no. 5, 055009, arXiv:1411.0535 \[hep-ph\]](#).
- [21] **ATLAS** Collaboration, G. Aad *et al.*, *Search for new phenomena in final states with an energetic jet and large missing transverse momentum in pp collisions at $\sqrt{s}=8$ TeV with the ATLAS detector*. [Eur. Phys. J. **C75** \(2015\) no. 7, 299, arXiv:1502.01518 \[hep-ex\]](#). [Erratum: *Eur. Phys. J.*C75, no.9, 408 (2015)].
- [22] **CMS** Collaboration, V. Khachatryan *et al.*, *Search for dark matter, extra dimensions, and unparticles in monojet events in protonproton collisions at $\sqrt{s}=8$ TeV*. [Eur. Phys. J. **C75** \(2015\) no. 5, 235, arXiv:1408.3583 \[hep-ex\]](#).
- [23] **IceCube** Collaboration, M. G. Aartsen *et al.*, *Improved limits on dark matter annihilation in the Sun with the 79-string IceCube detector and implications for supersymmetry*. [arXiv:1601.00653 \[hep-ph\]](#).
- [24] N. F. Bell, Y. Cai, J. B. Dent, R. K. Leane, and T. J. Weiler, *Dark matter at the LHC: Effective field theories and gauge invariance*. [Phys. Rev. **D92** \(2015\) no. 5, 053008, arXiv:1503.07874 \[hep-ph\]](#).
- [25] **ATLAS** Collaboration, G. Aad *et al.*, *Search for new phenomena in events with a photon and missing transverse momentum in pp collisions at $\sqrt{s}=8$ TeV with the ATLAS detector*. [Phys. Rev. **D91** \(2015\) no. 1, 012008, arXiv:1411.1559 \[hep-ex\]](#). [Erratum: *Phys. Rev.*D92,no.5,059903(2015)].
- [26] **CMS** Collaboration, V. Khachatryan *et al.*, *Search for new phenomena in monophoton final states in proton-proton collisions at $\sqrt{s}=8$ TeV*. [arXiv:1410.8812 \[hep-ex\]](#).
- [27] A. Alloul, N. D. Christensen, C. Degrande, C. Duhr, and B. Fuks, *FeynRules 2.0 - A complete toolbox for tree-level phenomenology*. [Comput.Phys.Commun. **185** \(2014\) 2250–2300, arXiv:1310.1921 \[hep-ph\]](#).
- [28] J. Alwall, R. Frederix, S. Frixione, V. Hirschi, F. Maltoni, *et al.*, *The automated computation of tree-level and next-to-leading order differential cross sections, and their matching to parton shower simulations*. [JHEP **1407** \(2014\) 079, arXiv:1405.0301 \[hep-ph\]](#).
- [29] T. Sjostrand, S. Mrenna, and P. Z. Skands, *PYTHIA 6.4 Physics and Manual*. [JHEP **0605** \(2006\) 026, arXiv:hep-ph/0603175 \[hep-ph\]](#).
- [30] **DELPHES 3** Collaboration, J. de Favereau *et al.*, *DELPHES 3, A modular framework for fast simulation of a generic collider experiment*. [JHEP **1402** \(2014\) 057, arXiv:1307.6346 \[hep-ex\]](#).
- [31] **UA2** Collaboration, J. Alitti *et al.*, *A Search for new intermediate vector mesons and excited quarks decaying to two jets at the CERN $\bar{p}p$ collider*. [Nucl. Phys. **B400** \(1993\) 3–24](#).
- [32] **CDF** Collaboration, T. Aaltonen *et al.*, *Search for new particles decaying into dijets in proton-antiproton collisions at $s^{1/2}=1.96$ -TeV*. [Phys. Rev. **D79** \(2009\) 112002, arXiv:0812.4036 \[hep-ex\]](#).
- [33] **ATLAS** Collaboration, T. A. collaboration, *Search for a dijet resonance produced in association with a leptonically decaying W or Z boson with the ATLAS detector at $\sqrt{s}=8$ TeV*.

- [34] **ATLAS** Collaboration, G. Aad *et al.*, *Search for new phenomena in the dijet mass distribution using $p - p$ collision data at $\sqrt{s} = 8$ TeV with the ATLAS detector*. [Phys. Rev. D](#) **D91** (2015) no. 5, 052007, [arXiv:1407.1376 \[hep-ex\]](#).
- [35] **CMS** Collaboration, V. Khachatryan *et al.*, *Search for resonances and quantum black holes using dijet mass spectra in proton-proton collisions at $\sqrt{s} = 8$ TeV*. [Phys. Rev. D](#) **D91** (2015) no. 5, 052009, [arXiv:1501.04198 \[hep-ex\]](#).
- [36] A. Belyaev, N. D. Christensen, and A. Pukhov, *CalcHEP 3.4 for collider physics within and beyond the Standard Model*. [Comput.Phys.Comm.](#) **184** (2013) 1729–1769, [arXiv:1207.6082 \[hep-ph\]](#).
- [37] G. Blanger, F. Boudjema, A. Pukhov, and A. Semenov, *micrOMEGAs4.1: two dark matter candidates*. [Comput.Phys.Comm.](#) **192** (2015) 322–329, [arXiv:1407.6129 \[hep-ph\]](#).
- [38] P. Gondolo and G. Gelmini, *Cosmic abundances of stable particles: Improved analysis*. [Nucl.Phys.](#) **B360** (1991) 145–179.
- [39] J.-M. Zheng, Z.-H. Yu, J.-W. Shao, X.-J. Bi, Z. Li, *et al.*, *Constraining the interaction strength between dark matter and visible matter: I. fermionic dark matter*. [Nucl.Phys.](#) **B854** (2012) 350–374, [arXiv:1012.2022 \[hep-ph\]](#).
- [40] H. Dreiner, M. Huck, M. Krämer, D. Schmeier, and J. Tattersall, *Illuminating Dark Matter at the ILC*. [Phys.Rev.](#) **D87** (2013) no. 7, 075015, [arXiv:1211.2254 \[hep-ph\]](#).
- [41] H. Goldberg, *Constraint on the Photino Mass from Cosmology*. [Phys.Rev.Lett.](#) **50** (1983) 1419.
- [42] H. Goldberg, *Erratum: Constraint on the Photino Mass from Cosmology*. [Phys. Rev. Lett.](#) **103** (2009) 099905.
- [43] **Planck** Collaboration, P. A. R. Ade *et al.*, *Planck 2013 results. XVI. Cosmological parameters*. [Astron. Astrophys.](#) **571** (2014) A16, [arXiv:1303.5076 \[astro-ph.CO\]](#).
- [44] K. Griest and M. Kamionkowski, *Unitarity Limits on the Mass and Radius of Dark Matter Particles*. [Phys. Rev. Lett.](#) **64** (1990) 615.
- [45] G. Jungman, M. Kamionkowski, and K. Griest, *Supersymmetric dark matter*. [Phys.Rept.](#) **267** (1996) 195–373, [arXiv:hep-ph/9506380 \[hep-ph\]](#).
- [46] K. Griest and D. Seckel, *Cosmic Asymmetry, Neutrinos and the Sun*. [Nucl. Phys.](#) **B283** (1987) 681. [Erratum: [Nucl. Phys.](#) **B296**, 1034 (1988)].
- [47] **IceCube** Collaboration, M. Aartsen *et al.*, *Search for dark matter annihilations in the Sun with the 79-string IceCube detector*. [Phys.Rev.Lett.](#) **110** (2013) no. 13, 131302, [arXiv:1212.4097 \[astro-ph.HE\]](#).
- [48] P. Agrawal, Z. Chacko, C. Kilic, and R. K. Mishra, *A Classification of Dark Matter Candidates with Primarily Spin-Dependent Interactions with Matter*. [arXiv:1003.1912 \[hep-ph\]](#).
- [49] C. Savage, A. Scaffidi, M. White, and A. G. Williams, *LUX likelihood and limits on spin-independent and spin-dependent WIMP couplings with LUXCalc*. [arXiv:1502.02667 \[hep-ph\]](#).

- [50] H.-Y. Cheng and C.-W. Chiang, *Revisiting Scalar and Pseudoscalar Couplings with Nucleons*. [JHEP **07** \(2012\) 009](#), [arXiv:1202.1292 \[hep-ph\]](#).
- [51] G. Wikstrom and J. Edsjo, *Limits on the WIMP-nucleon scattering cross-section from neutrino telescopes*. [JCAP **0904** \(2009\) 009](#), [arXiv:0903.2986 \[astro-ph.CO\]](#).
- [52] J. N. Bahcall, A. M. Serenelli, and S. Basu, *New solar opacities, abundances, helioseismology, and neutrino fluxes*. [Astrophys. J. **621** \(2005\) L85–L88](#), [arXiv:astro-ph/0412440 \[astro-ph\]](#).
- [53] P. Gondolo, J. Edsjo, P. Ullio, L. Bergstrom, M. Schelke, and E. A. Baltz, *DarkSUSY: Computing supersymmetric dark matter properties numerically*. [JCAP **0407** \(2004\) 008](#), [arXiv:astro-ph/0406204 \[astro-ph\]](#).
- [54] M. Blennow, J. Edsjo, and T. Ohlsson, *Neutrinos from WIMP annihilations using a full three-flavor Monte Carlo*. [JCAP **0801** \(2008\) 021](#), [arXiv:0709.3898 \[hep-ph\]](#).
- [55] J. Edsjo, *Nusigma*. <http://copsosx03.fysik.su.se/wimpsim/code/nucross3.pdf>.
- [56] D. V. Forero, M. Tortola, and J. W. F. Valle, *Global status of neutrino oscillation parameters after Neutrino-2012*. [Phys. Rev. **D86** \(2012\) 073012](#), [arXiv:1205.4018 \[hep-ph\]](#).
- [57] **LUX** Collaboration, D. S. Akerib *et al.*, *First results from the LUX dark matter experiment at the Sanford Underground Research Facility*. [Phys. Rev. Lett. **112** \(2014\) 091303](#), [arXiv:1310.8214 \[astro-ph.CO\]](#).